α-Al_2O_3 sapphire and rubies deformed by dual basal slip at intermediate temperatures (900°C-1300°C). I – Dislocation organization

M. Castillo Rodríguez*, J. Castaing, A. Muñoz*, P. Veyssière*** and A. Domínguez Rodríguez***

*Departamento Física de la Materia Condensada. Universidad de Sevilla, anmube@us.es. Apdo. 1065, 41080 Seville (Spain)

**C2RMF, CNRS UMR 171, jacques.castaing@culture.fr. Palais du Louvre, 14 quai François Mitterrand 75001 Paris (France)

***LEM, CNRS UMR 104, ONERA, BP 72, 92322 CHATILLON Cedex (France)

Abstract: Under a load orientation that hinders twinning and impedes fracture, sapphire and Cr-doped α-Al_2O_3 single crystals (rubies) were deformed from 1500 ºC to slightly above the brittle to ductile transition temperature of 900°C. deformed from 1500 ºC to slightly above the brittle to ductile transition temperature of 900°C. Transmission electron microscope observations of dislocation structures in rubies and sapphire deformed at 1000°C and at 1300°C show features such as long straight segments, dipoles and loops whose formation mechanisms are discussed. The operation of two $<1\bar{1}20>$ glide directions in the basal plane promotes specific, temperature-dependent dislocation reactions, including "pseudo-dipoles" formed by attractive dislocations with different Burgers vectors. At the lowest temperatures explored, the deformation structure comprises a large density of straight dislocation segments along $<\bar{1}2\bar{1}0>$ and $<\bar{1}010>$ directions typical of a Peierls-controlled dislocation motion, that supports recent modelling of the temperature dependence of the CRSS. The companion paper (part II) deals with dislocation fine structure and in particular with the mechanisms involved in the formation of a variety of faulted debris.

* Corresponding author. Tel.: +34-95-455-0939; fax: +34-95-461-2097.
E-mail address: anmube@us.es (A. Muñoz).
Keywords: sapphire, ruby, dislocation microstructure, basal slip, Peierls mechanism.

1. Introduction

Defects engendered by plastic deformation in α-Al_2O_3 single crystal (sapphire) have been examined by transmission electron microscopy (TEM) over several decades [1, 2]. Basal slip is the deformation mode that has been most often investigated in specimens orientated to provide a maximum Schmid factor for one such slip system with the compression direction at 45° from the slip plane and $1/3 < 1\bar{2}10 >$ Burgers vector, the so-called *a* orientation [3]. These studies were, however, restricted to high temperatures (T > 1400°C) at which the flow stress for basal slip is smaller than that for rhombohedral twinning. Basal slip could be activated below 800°C under a hydrostatic pressure of 1.5 GPa [4] itself necessitated by the intrinsic brittleness of sapphire at ambient pressure below 900°C. The density of twins and dislocations was then so high that TEM could not provide useful information on dislocation-mediated strain [4]. It is only recently that was tested another orientation, the so-called *aa* orientation, that both hinders rhombohedral twinning and activates basal slip in sapphire and rubies (Cr doped α-Al_2O_3) at ambient pressure an temperatures between 900°C and 1300°C [3, 5, 6], thus lower than in previous studies conducted under the *a*-orientation [2, 7-9]. In practice, the compression axis lies at about 60° from the [0001] direction near the $[\bar{2}021]$ direction in the $(1\bar{2}10)$ plane and is such that two families of dislocations experience about the same resolved shear stress [3].

The present work embraces an investigation of the structure of dislocations introduced near the ductile to brittle transition of sapphire and rubies (T = 900 – 1000°C) together with an analysis of the dislocation processes associated with the operation of two Burgers vectors confined to parallel slip planes. Dislocation mechanisms involved

during deformation are also analyzed in relation with a kink pair model that describes the dependence of the critical resolved stress (CRSS) with the temperature [5, 6].

2. Experimental procedure

Sapphire and four different types of rubies grown by the Verneuil technique were provided by R.S.A Le Rubis (Jarrie, France). Impurity concentrations were determined by PIXE at CNA (Seville-Spain) and at C2RMF-CNRS (Paris-France), to be below 11 ppm mol of Ni, Cu, Ga, Co, Zn, V, slightly greater for Ti, and 60, 725, 3940 and 9540 ppm mol of Cr^{3+} as average values for the ruby specimens .[5] Compression tests were performed in air at constant strain rate ($\dot{\varepsilon} \approx 2 \cdot 10^{-5}\ s^{-1}$) and temperatures between 900 and 1500 ºC [3, 5]. Under the *aa*-orientation, the two basal slip directions, $\mathbf{b}_1 = 1/3\,[1\bar{1}20]$ and $\mathbf{b}_2 = 1/3\,[\bar{2}110]$, are subjected to a Schmid factor of about 0.4 [3]. The experimental procedures used in the tests and their results can be found in previous papers [3, 5]. The TEM investigation of the influence of Cr^{3+} on the dislocation microstructure of sapphire was conducted on specimens of sapphire either undoped or doped with low (725 ppm mol) and high (9540 ppm mol) concentrations of Cr^{3+} and deformed at 1000 and 1300ºC. Foils with different orientations were cut out of each deformed specimen including one parallel to the basal plane (0001). In the latter, foils exhibited dislocation lines meandering uninterruptedly over 5 to 10 µm, thus providing a fair account of the expansion and organization of dislocations in their own slip plane. This foil orientation facilitates the identification of all the Burgers vectors of perfect and partial basal dislocations via a standard $\mathbf{g}\cdot\mathbf{b}$ analysis. All the foils were mechanically ground to a thickness of about 100 µm and subsequently polished with diamond pastes down to 3 µm in grain size. They were then dimpled to ~30 µm in thickness (Dimpler

grinder Gatan Model-656) and ion-thinned to electron transparency with argon ions in a PIPS Gatan Model-691 apparatus operated at 5 kV with the incidence angle gradually decreased from 10º to 4º, and finally at 4 kV and 4º to minimize ion damage. A thin carbon coating was deposited on the foils by vacuum evaporation to prevent charge buildup during observation in the electron microscope. The specimens were examined under diffraction contrast by the weak-beam technique, which is best suited to analyze the dislocation fine structure on reasonably long segments, with a Jeol 200 CX electron microscope (Laboratoire d'Etude des Microstructures, CNRS-ONERA, France) and a Hitachi H-800 (CITIUS, Spain), both operating at 200 kV. Imaging plates were used to record most images as they help diminish exposure time considerably (from 30 sec to 1-2 sec in weak beam) thus reducing difficulties associated with sample drifting.

3. Results and discussion

The stress-strain curves display a yield peak followed by a work-hardened stage [5, 6]. The present TEM work focuses on dislocation properties at the lower yield point corresponding to a permanent strain of about 2%. In every sample investigated, the microstructure of deformation in the *aa* orientation is as expected dominated by dislocations with the two Burgers vectors $\mathbf{b_1} = 1/3\,[1\bar{2}10]$ and $\mathbf{b_2} = 1/3\,[\bar{2}110]$ which are present under comparable proportions [3]. Figure 1 illustrates the property that regardless of Cr^{3+} concentration, sapphire and rubies deformed under the *aa* orientation show the typical microstructural elements previously reported in sapphire [2, 8-11], i.e. dislocations segmented along specific orientations, unfaulted dipoles (PD) and loops (PL) as well as faulted dipoles (FD) and loops (FL). The main difference between the present and previous observations relies in the numerous dislocation reactions, not found before since

then only one glide direction was activated against two coplanar here. The features observed in Figure 1 will be commented throughout this paper and the faulted debris will be analyzed and their origin discussed in the companion paper (part II).

3.1 Peierls effects

The TEM samples of *aa*-oriented sapphire deformed to ε = 1.7% by basal slip at 1252 ºC and maintained under 451 MPa at 804 ºC for 200 min, exhibit conspicuous evidence of the effects of the Peierls mechanism under the form of a relatively large density of long straight segments (Figure 2), thus revealing two crystallographically distinct Peierls potential minima. The TEM samples of rubies deformed at 1000°C under the *aa* orientation show dislocation arrangements similar to those encountered in sapphire, including clear evidence of Peierls-controlled configurations [5]. Observations achieved on several samples all indicate that the favored dislocation orientations lie essentially along the mixed 30º $<\bar{1}010>$ and 60º $<1\bar{2}10>$ directions, coexisting with a minor fraction of edge $<\bar{1}010>$ dislocations. Screw segments along $<11\bar{2}0>$ are also observed in places but in comparatively small proportions. In a foil prepared from a sample deformed in single slip (*a*-orientation) and sliced parallel to the basal slip plane, Lagerlof *et al.*[4] reported that most dislocations introduced at 800°C and under hydrostatic pressure, lie along $<\bar{1}010>$ directions, hence of either mixed 30º or edge character. The finding of favored $<\bar{1}010>$ directions is at variance from the present results. In part II (§ 2.1), we show that the stabilization of segments along ± 30° $<\bar{1}010>$ directions is consistent with a potential core extension of basal dislocations.

In the context of a Peierls model based on dislocation glide controlled by the nucleation and propagation of kink pairs [5], one should distinguish between two situations. In the *short segment approximation*, the nucleation rate of kink pairs is low

enough for the kinks to slide unhindered over the full dislocation line resulting in straight dislocation lines. On the other hand, kink pair nucleation occurs more frequently in the *long segment approximation* with the kinks then impacting each other, annihilating or combining to form macrokinks before they can attain the extremities of the segment under consideration, and forcing this segment to a certain curvature under load. Upon unloading though, dislocations may reorient along the directions where the Peierls potential is a minimum which makes it difficult distinguishing between the *short* and the *long segment* limits, based on the observation of segments along crystallographic directions in *post mortem* samples. In the present case though, the observations of relatively long rectilinear dislocations (Figure 2) strongly suggest the operation of the *long segment mechanism*, as concluded in a previous work [5].

3.2. Dislocation dipoles and pseudo dipoles

Elongated dipoles edge or mixed 60º in character, exceeding 5 μm in length were currently observed together with *pseudo dipoles* comprised of two attractive dislocations with different Burgers vectors.

The simplest way to think of dipole and pseudo-dipole formation in basal slip is to consider two sources of dislocations operating in nearby planes. Whatever their relative orientations and positions, these sources will produce repulsive and attractive configurations which are stable if the distance between the two basal slip planes, the dipole height, is less than a critical distance that depends on the applied shear stress. The maximum dipole heights of about 0.15 μm observed after deformation at 1300°C corresponds with a calculated passing stress of 20.5 MPa consistent with the resolved flow stress of 30 MPa measured at this temperature. Pseudo dipoles, are rather frequently observed in the 1000-1050° range in deformed sapphire and ruby essentially because no

slip systems other than the two slip directions in the basal plane are activated under the *aa* orientation. As discussed hereafter, cross-slip activity on prism and pyramidal planes is indeed relatively modest. Pseudo dipoles are actually scarce in systems with higher symmetry owing to the multiplicity of equivalent slip systems and to the resulting dislocation reactions. A notable exception is that of cubic γ-TiAl owing to the existence of several non-equivalent slip directions per {111} slip plane [12].

Pseudo dipoles exhibit elastic properties which differ substantially from those of dipoles [13]. These properties can be characterized in terms of two parameters, the equilibrium angle and the passing stress, both calculated here under anisotropic elasticity (elastic constants from reference [14]). The equilibrium angle of a dipolar configuration is the angle between the slip plane and the habit plane of the dislocation partners. It is plotted in Figure 3(a) which is generic in sapphire owing to the invariance of the configurations with respect to a rotation of 120°. For simplicity, the origin of the dislocation character θ, is identified to the screw orientation of one given dislocation (lower horizontal axis) and for a pseudo dipole the character of the other dislocation is chosen as $\theta + 120°$ (upper horizontal axis). The minimum pseudo dipole equilibrium angle amounts to ±38° for the dislocation character of $\theta = 120°$ (the same angle as for a pseudo dipole with $\theta = 60°$ and second dislocation with character of $\theta - 120°$). By comparison, the minimum equilibrium angle of a dipole in sapphire which is elastically isotropic is reached in the edge orientation and amounts to -45° as is expected. For $-10° < \theta < 70°$ the equilibrium angle of the pseudo dipole is 90° (for $170° < \theta < 250°$ in the case of the other pseudo dipole).

Since interaction stresses are proportional to the scalar product of the interacting Burgers vectors, the passing stress of a pseudo dipole with given height, that is, the

applied shear stress above which it is no longer stable, is always less than that of a dipole. This is shown in Figure 3(b) for a dipole and a pseudo dipole with the same height of 30*b*, where $b = 4.75\ 10^{-10}$ nm is the magnitude of the perfect basal Burgers vector. For the pseudo dipole, the maximum passing stress, which is attained for $\theta = 30°$, is decreased by about 20% with respect to that of the dipole ($\theta = 0°$). The minimum passing stress is decreased by a factor of 2. Since it is in its weakest part that a dipole should yield under the applied stress, it is clear that the contribution of pseudo dipoles of perfect dislocations to hardening is insignificant compared to that of dipoles.

The observation of pseudo dipolar configurations is, however, often obscured due to further interactions with impacting dislocations and their accumulation. One example is given in Figure 1(a) for sapphire with two pseudo dipoles, the long oblique one in the middle of the micrograph interacting with a third dislocation. Figure 4(a) shows an elongated composite dipolar feature in sapphire deformed at 1050°C that originates from a dipole of 30° mixed dislocations with Burgers vector $\pm \mathbf{b}_2$ (= $1/3[\bar{2}110]$). In the central section of this feature lies a *pseudo dipole* in which one portion of the parent dipole is associated with an edge $\mathbf{b}_3$ (= $1/3[\bar{1}2\bar{1}0]$) dislocation. Nearly aligned with $[10\bar{1}0]$, the pseudo dipole is delimited by two nodes each comprising a branch of $\mathbf{b}_1$ (= $1/3[11\bar{2}0]$) dislocation and a dipole of $\mathbf{b}_2$ dislocations. The pseudo dipole was thus formed by the reaction between one component of the $\pm\mathbf{b}_2$ parent dipole and an impacting $\mathbf{b}_1$ dislocation. The final shape adopted by the various components of this complex configuration reflects prior dynamical interactions with mobile dislocations whose analysis is beyond reach. The dipole heights are smaller for pseudo dipoles (≈ 20nm) than for dipoles (≈ 30nm) in agreement with the dipole binding forces being comparatively larger in dipoles than in pseudo dipoles. The habit plane of the three dipole branches lies near a plane at

approximately 60° from (0001) which, according to Figure 3(a), is 30° away from the equilibrium configuration for the pseudo dipole, and not far from equilibrium for the edge and 60° dipoles (45° and 55° respectively).

In Figure 4(b) taken from 725 ppm Cr^{3+} ruby deformed at 1000°C, a dislocation with Burgers vector $\mathbf{b}_3 = 1/3[\bar{1}2\bar{1}0]$ was able to accommodate two different pseudo-dipolar portions along its line. The pseudo dipole PS-1 is comprised of a 60° segment of the $\mathbf{b}_3$ dislocation associated with a screw $\mathbf{b}_2$ dislocation. The other pseudo-dipole PS-2 involves a screw portion of the $\mathbf{b}_3$ dislocation and a $\mathbf{b}_1$ 60° dislocation. That the screw segments in each pseudo dipole have not cross-slipped to form a junction with its partner reflects a high lattice friction both in the pyramidal plane during the approach and in the prism plane at dipole equilibrium. There are two possible prism planes, i.e. $\{10\bar{1}0\}$ which could be involved in the cross-slip reaction forming the junction, and $\{\bar{1}2\bar{1}0\}$ which is observed [1, 2, 4]. The CRSS of 90 MPa in pyramidal slip at 1750°C [15] is not excessively high, i.e. about twice that of $\{\bar{1}2\bar{1}0\}$ slip [2, 4]. It is a plausible cross-slip plane for a $1/3<11\bar{2}0>$ dislocation.

3.3. Oriented loops.

In sapphire and rubies deformed at 1000-1050°C, the presence of *oriented* loops and hairpins of perfect dislocations such as shown in Figure 5 attests to the dominance of glide-mediated transformation processes (see also feature B in Figure 1(a)). Such debris are comprised of a succession of loops such that one extremity of a given loop is aligned with the extremity of a neighboring loop along the Burgers vector direction. Similar debris has been identified in [16, 17]. They are generated in places by cross-slip annihilation of the screw portions of meandering dipoles, thus explaining the specific

orientation relationship. It is worth emphasizing that this orientation relationship has no equivalence in climb-mediated dipole pinching off since the latter, which may occur anywhere on mixed segments [18], results in loop extremities aligned in whatever orientation but screw. It is noted that the mixed prismatic loops formed by cross-slip annihilation flip to their minimum energy configuration, the edge prismatic loop, by glide on their composite prism/basal glide surface which is defined by their Burgers vector and their line. In passing, the observation of oriented loops confirms that cross-slip may operate in sapphire under large enough driving stresses as is the case for small dipole heights (≈25 nm) observed after deformation around 1000°C, and contrary to the situation exemplified in Figure 4 where cross-slip was not active. An estimate of the corresponding driving stress is obtained from the stress field exerted by a screw dislocation $\frac{\mu b}{2\pi r}$ which, with μ = 156 GPa for sapphire and $r = 50b$ yields about 500 MPa. Since the observed dipole width of 50*b* may not be the largest, 500 MPa overestimates of the critical shear stress to activate cross-slip annihilation at this temperature. As discussed above annihilation should take place via a pyramidal cross-slip plane. Oriented dipoles and loops are formed in both undoped and Cr^{+3} doped sapphire at low temperature (1000 – 1100°C).

3.4. Dislocation reactions

Beside the two above-mentioned Burgers vectors $\mathbf{b_1} = 1/3[11\bar{2}0]$ and $\mathbf{b_2} = 1/3[\bar{2}110]$, the presence in places of the third basal Burgers vector $\mathbf{b_3} = 1/3[\bar{1}2\bar{1}0]$, whose Schmid factor is nil, attests to the reaction of the two $\mathbf{b_1}$ and $\mathbf{b_2}$ slip directions (Figure 1). Unless two dislocations with Burgers vectors $\mathbf{b}_1$ and $\mathbf{b}_2$ lie in exactly the same basal plane, they will interact forming dipoles or pseudo dipoles (sections 3.2 and 3.3),

and they may react either by cross-slip at the lowest test temperatures or by climb when temperature is high enough. When temperature enables diffusion, a pseudo dipole of any character may evolve and transform either partly to give a faulted pseudo dipole of partial dislocation (see part II), or fully thus forming a single junction segment with Burgers $\mathbf{b}_3$. The proportion of such junctions relative to pseudo dipoles provides an indication of the climb activity during deformation.

As regards cross-slip, which is the prominent degree of freedom at the lowest temperatures investigated here, a reaction can occur along either one of the two screw directions defined by $\mathbf{b}_1$ and $\mathbf{b}_2$ producing a junction delimited by two nodes along this direction. In Figure 1.b for instance, which was taken from a foil deformed at 1300°C, the two nodes of dislocation 3 are aligned with the Burgers vector of dislocation 1, attesting that the latter had cross-slipped. By contrast, dislocation 6 is aligned with the Burgers vector of neither dislocation 5 nor dislocation 4, implying a diffusion-mediated reaction. The same conclusion applies to the $\mathbf{b}_3$ junction in Figure 1(a) that was probably formed at 1250°C. The final product of dislocation reaction depends strongly on test temperature as one dislocation in ten displays a node at 1000ºC whereas one in three displays a node at 1300ºC. The presence of unfaulted (PD in Figure 1(a)) and faulted dipoles, (FD, Figure 1(b)) and loops (PL and FL) is consistent with previous investigations on *a*-oriented samples [9]. Properties of faulted features are discussed separately in part II.

4. Concluding remarks

The microstructure of deformation of sapphire and ruby has been investigated for a load orientation (*aa*) that differs from that (*a* orientation) usually adopted so far. The *aa* orientation activates two basal slip directions in twin-free samples above a temperature as low as 900°C, thus enabling analysis of properties of individual dislocations over a

much wider temperature range than for the *a* orientation. Samples deformed around 1000°C to the lower yield point are dominated by dislocations elongated in the $\pm 30° < \bar{1}010 >$ and $60º < 1\bar{2}10 >$ directions typical of a Peierls mechanism and suggesting deformation operating in the so-called *long segment limit*. Below 1300°C, the two slip directions form dipole and pseudo dipoles whose respective elastic properties (equilibrium angle and passing stresses) exhibit significant differences. Above 1300°C, dipoles and pseudo dipoles annihilate or form junctions, respectively. Dislocations with the third basal Burgers vector are a good indicator of the extent to which cross-slip and climb have operated. Chromium has a negligible influence on the deformation microstructure.

Acknowledgements

This work has been supported by the Ministry of Science and Technology (Government of Spain) through the project MAT2003-04199-CO2-02.

Figure captions

Figure 1 : (a) Dislocation microstructure of sapphire deformed to $\varepsilon = 2\%$ at 1250°C and 1.5% at 1050°C (final applied stress = 286 MPa) by basal slip. Dislocation elongation along dense directions of the basal plane should be noted together with, at B, the alignment in the $[11\bar{2}0]$ direction of the tips of the two hairpins (dipoles of perfect dislocation (PD) with Burgers vector $\mathbf{b}_1 = 1/3[11\bar{2}0]$). Crossing the figure obliquely is a "pseudo-dipole" formed by two $\mathbf{b}_1$ and $\mathbf{b}_2$ (= $[\bar{2}110]$) dislocations in its lower portion, and a threefold configuration including $\mathbf{b}_1$, $\mathbf{b}_2$ and $-\mathbf{b}_1$ in its upper part. Bottom left, a near-screw $\mathbf{b}_3$ (= $[\bar{1}2\bar{1}0]$) junction between two nodes resulting from the reaction of two dislocations with Burgers vectors $\mathbf{b}_1$ and $\mathbf{b}_2$ arranged as a "pseudo-dipole" at the upper left end. The junction is in contrast under $\mathbf{g} = \bar{3}300$ (insert).

(b) Dislocation microstructure of sapphire doped with 9540 mol ppm of Cr^{3+}, deformed to $\varepsilon = 2\%$ at 1300 ºC by basal slip. The foil is normal to [0001] direction and it shows reactions or junctions between dislocations (R), faulted dipoles (FD), and unfaulted and faulted loops (PB, FB). The dislocation segments labelled {1, 5}, {2, 4}, {3, 6, R, PL} and FL have Burgers vectors $\mathbf{b}_1$, $\mathbf{b}_2$, $\mathbf{b}_3$ and $1/3[1\bar{1}00]$, respectively.

Figure 2 : Sapphire deformed to $\varepsilon = 1.7\%$ by basal slip at 1252 ºC and maintained under 451 MPa at 804 ºC for 200 min at the end of the test. The foil is normal to [0001] direction is inclined by 14°, and the straight segment of dislocation lines along simple crystallographic directions is a clear evidence of Peierls mechanism. Angles measured between rectilinear segments are indicated. Horizontally, the micrograph spans 25 μm.

Figure 3 : Equilibrium angle and passing stress for dipoles (dashed lines) and for pseudo-dipoles (full line) as a function of the dipole character (c_{11} = 497.5 GPa, c_{33} = 503.3 GPa, c_{12} = 162.7 GPa, c_{13} = 115.5 GPa, c_{44} = 147.4 GPa, c_{14} = 22.5 GPa [14]). More details on the calculation including an approximate expression of the passing stress under isotropic elasticity can be found in [13].

Figure 4 : In order to enhance visibility, the contrast of both micrographs, taken under dark field weak beam conditions, has been reversed. (a) sapphire deformed first at 1250°C and at 1050°C and (b) ruby doped with 725 mol ppm of Cr^{3+} deformed at 1000°C. The foils are close to basal plane. The central part of (a) is crossed by a 4.5 µm long dipolar feature presenting from left to right: 0.25µm faulted dipole (see upper left inset), 1 µm dipole, 1.6 µm pseudo dipole and 2 µm dipole, the last two are parallel to [10$\bar{1}$0]. Dipoles and pseudo-dipoles can also be seen in (b). The perfect dipole noted PD_2, which is viewed under **g.b** = 0 conditions, exhibits a residual contrast. Its width is therefore largely insensitive to the sign of $s_{\mathbf{g}}$ (bottom-right insert).

Figure 5 : Ruby doped with 9540 mol ppm of Cr^{3+} deformed by basal slip at 1000ºC showing oriented loops (the extremities of two consecutive loops are aligned in the [2$\bar{1}\bar{1}$0] direction.

References

[1] Heuer AH, Lagerlof KPD, Castaing J. Philos Mag A 1998;78:747
[2] Mitchell TE, Heuer AH. Dislocations and mechanical properties of ceramics. Dislocations in Solids, vol. Volume 12. Amsterdam: Elsevier, 2005. p.339.
[3] Castaing J, Muñoz A, Gomez Garcia D, Dominguez Rodriguez A. Materials Science and Engineering A 1997;233:121.
[4] Lagerlöf KPD, Heuer AH, Castaing J, Rivière JP, Mitchell TE. Journal of the American Ceramic Society 1994;77:385.
[5] Castillo Rodriguez M, Castaing J, Munoz A, Veyssière P, Dominguez Rodriguez A. Journal of the American Ceramic Society 2008;91:1612.
[6] Castillo Rodriguez M, Munoz A, Castaing J, Veyssière P, Dominguez Rodriguez A. Journal of the European Ceramic Society 2007;27:3317.
[7] Phillips DS, Mitchell TE, Heuer AH. Philos Mag A 1982;45:371
[8] Pletka BJ, Heuer AH, Mitchell TE. Acta Metallurgica 1977;25:25.
[9] Pletka BJ, Mitchell TE, Heuer AH. Acta Metallurgica 1982;30:147.
[10] Lagerlöf KDP, Pletka BJ, Mitchell TE, Heuer AH. Radiation Effects 1983;74:87.
[11] Mitchell TE, Pletka BJ, Phillips DS, Heuer AH. Philos Mag 1976;34:441
[12] Grégori F, Veyssière P. Philos Mag A 2000;80:2913.
[13] Veyssière P, Chiu YL. Philos Mag 2007;87:3351
[14] Gladden JR, So JH, Maynarda JD, Saxe PW, Le Page Y. 2004;Applied Physics Letters:392.
[15] Tressler RE, Barber DJ. Journal of the American Ceramic Society 1974;57:13.
[16] Shi X, Saada G, Veyssière P. Philos Mag Lett 1995;71:1
[17] Veyssière P, Grégori F. Philos Mag A 2002;82:567.
[18] Grégori F, Veyssière P. Philos Mag A 2002;82:553.

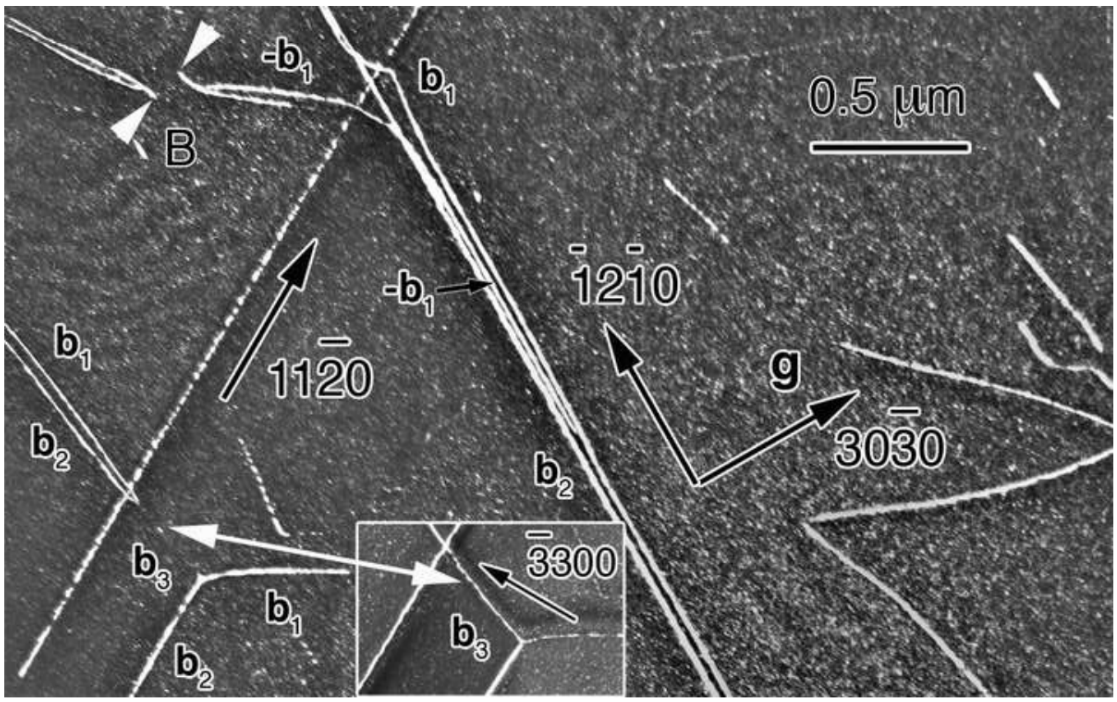

Figure 6a

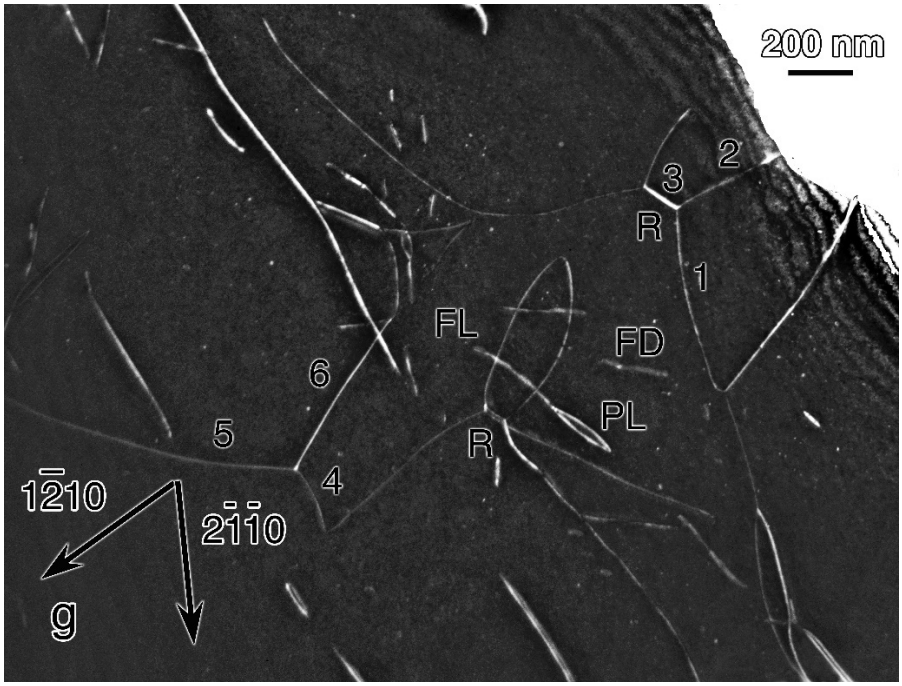

Figure 1 b

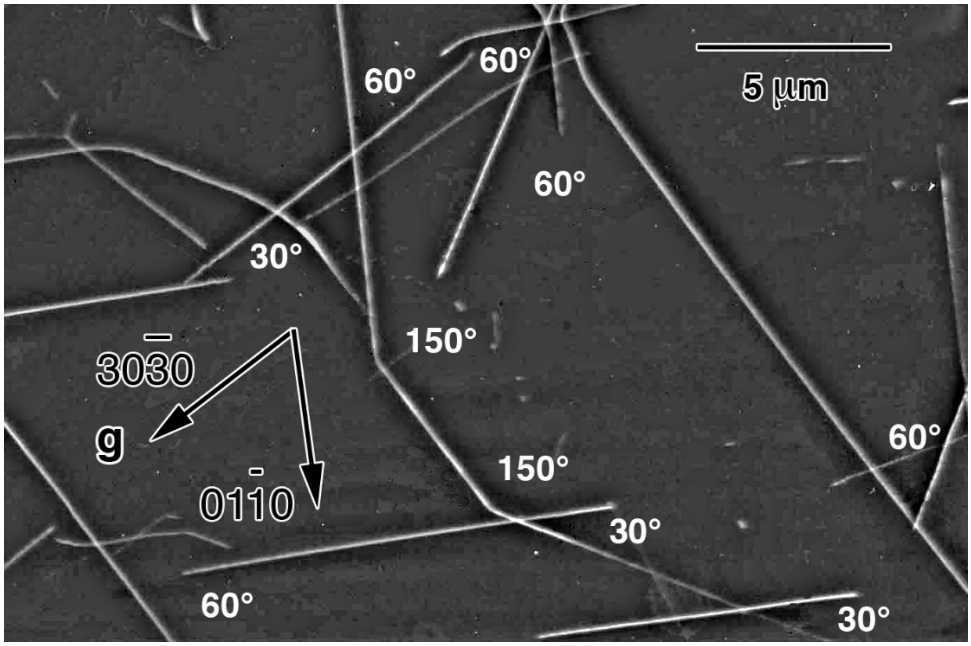

Figure 2

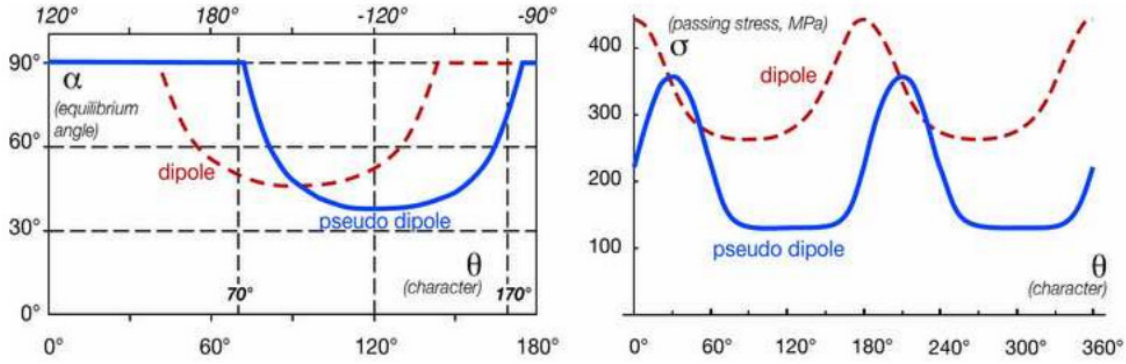
120°
180°
-120°
-90°
90°
α
(equilibrium angle)
60°
dipole
30°
pseudo dipole
θ
(character)
0°
70°
170°
0°
60°
120°
180°
(passing stress, MPa)
σ
400
300
200
100
dipole
pseudo dipole
θ
(character)
0°
60°
120°
180°
240°
300°
360°

Figure 3

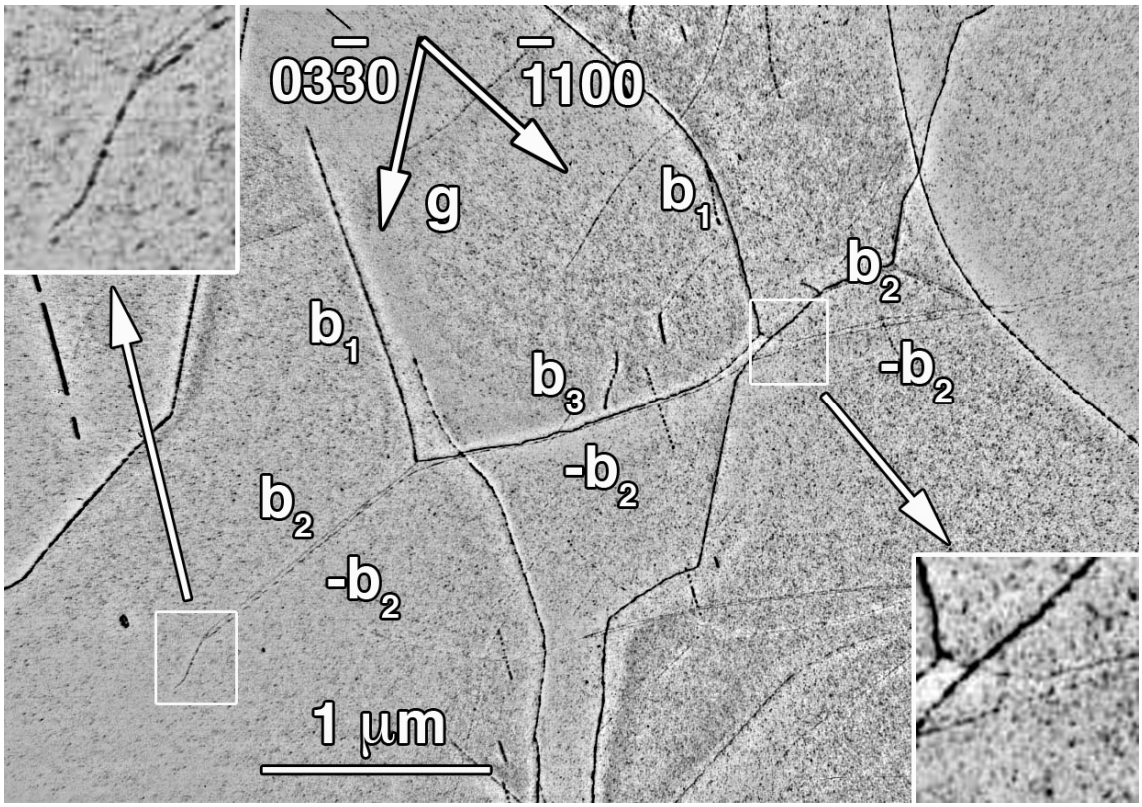

Figure 4

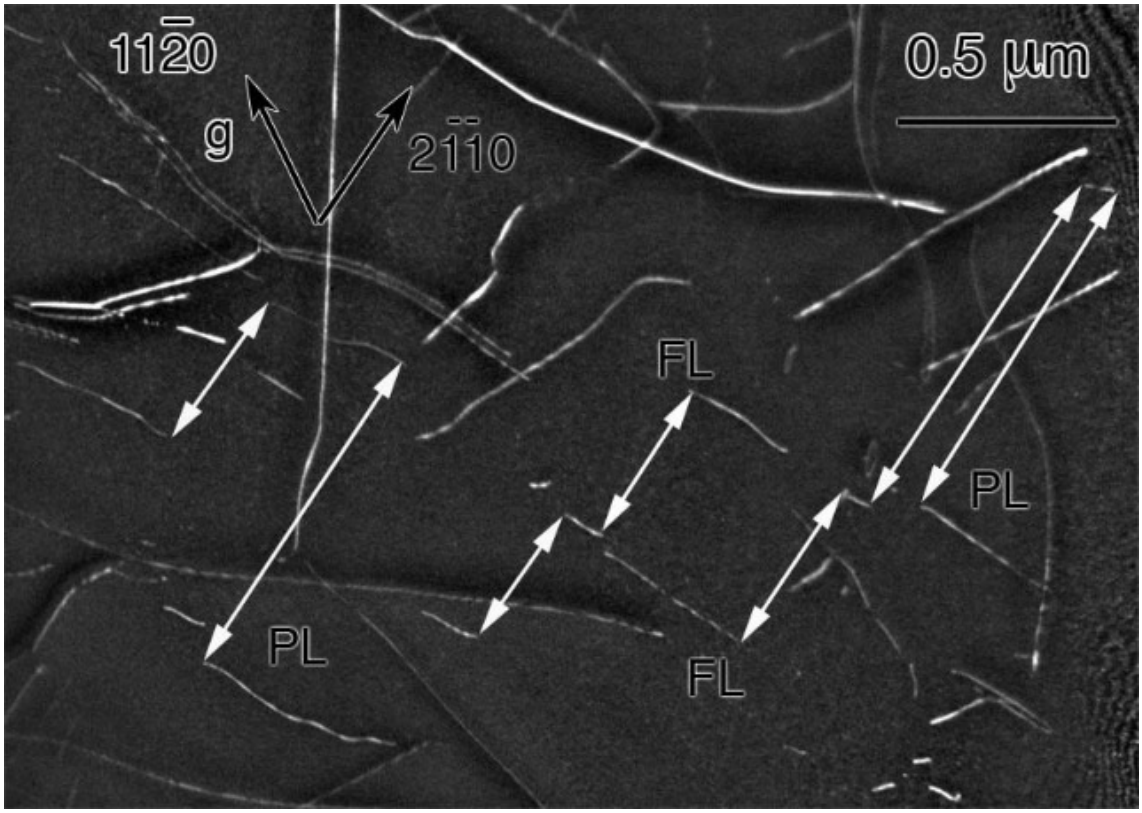

Figure 5